Contrib Mineral Petrol (1998) 131: 39–53

Lang Shi · Don Francis · John Ludden
Andrew Frederiksen · Michael Bostock

Xenolith evidence for lithospheric melting above anomalously hot mantle under the northern Canadian Cordillera

Received: 16 May 1997 / Accepted: 25 October 1997

Abstract A comparison of mantle xenolith suites along the northern Canadian Cordillera reveals that the xenoliths from three suites exhibit bimodal populations whereas the xenoliths from the other four suites display unimodal populations. The bimodal suites contain both fertile lherzolite and refractory harzburgite, while the unimodal suites are dominated by fertile lherzolite xenoliths. The location of the three bimodal xenolith suites correlates with a newly discovered P-wave slowness anomaly in the upper mantle that is 200 km in width and extends to depths of 400–500 km (Frederiksen AW, Bostock MG, Van Decar JC, Cassidy J, submitted to Tectonophysics). This correlation suggests that the bimodal xenolith suites may either contain fragments of the anomalously hot asthenospheric mantle or that the lithospheric upper mantle has been affected by the anomalously hot mantle. The lherzolite xenoliths in the bimodal suites display similar major element compositions and trace element patterns to the lherzolite xenoliths in the unimodal suites, suggesting that the lherzolites represent the regional lithospheric upper mantle. In contrast, the harzburgite xenoliths are highly depleted in terms of major element composition, but their clinopyroxenes [Cpx] have much higher incompatible trace element contents than those in the lherzolite xenoliths. The major element and mildly incompatible trace element systematics of the harzburgite and lherzolite xenoliths indicate that they could be related by a partial melting process. The lack of textural and geochemical evidence for the former existence of garnet argues against the harzburgite xenoliths representing actual fragments of the deeper anomalous asthenospheric mantle. Furthermore, the calculated P-wave velocity difference between harzburgite and lherzolite end-members is only 0.8%, with the harzburgites having higher P-wave velocities. Therefore the 3% P-wave velocity difference detected teleseismically cannot be produced by the compositional difference between the lherzolite and harzburgite xenoliths. If temperature is responsible for the observed 3% P-wave velocity perturbation, the anomalous mantle is likely to be at least 200 °C higher than the surrounding mantle. Taken together these data indicate that the refractory harzburgite xenoliths represent the residue of 20–25% partial melting of a lherzolite lithospheric mantle. The incompatible trace element enrichment of the harzburgites suggests that this melting was accompanied by the ingress of fluids. The association of the bimodal xenolith suites with the mantle anomaly detected teleseismically suggests that anomalously hot asthenospheric mantle provided both the heat and volatiles responsible for the localized melting and enrichment of the lithospheric mantle.

L. Shi · D. Francis (✉)
Earth and Planetary Sciences, McGill University,
3450 University St., Montreal, Quebec, H3A 2A7 Canada

J. Ludden[1]
Département de Géologie, Université de Montréal,
C.P. 6128, suc. "A", Montréal, Québec, H3C 3J7 Canada

A. Frederiksen · M. Bostock
Department of Earth and Ocean Science,
The University of British Columbia, 6339 Stores Road,
Vancouver, British Columbia, V6T 1Z4 Canada

Present address:
[1] CNRS/CRPG, 54501 Vandoeuvre-les-Nancy, BP 20, France

Editorial responsibility: T.L. Grove

Introduction

There is considerable controversy about whether the continental lithospheric mantle can significantly be melted by the ingress of heat and fluids from underlying mantle hot spots such as rising plumes (e.g. Hawkesworth et al. 1990; Gallagher and Hawkesworth 1992; Arndt and Christensen 1992; Arndt et al. 1993; Turner et al. 1996). Mantle xenoliths brought to the surface by alkaline basalts come from depths of 30–80 km and therefore represent actual samples of the lithospheric mantle and potentially retain evidence of previous melting events within the lithosphere. In this paper we report xenolith evidence for lithospheric melting beneath

the northern Canadian Cordillera in response to an underlying region of anomalously hot asthenospheric mantle.

We show that there are two types of xenolith suites along the northern Canadian Cordillera; bimodal suites that have both fertile lherzolite and refractory harzburgite xenoliths, and unimodal suites composed mainly of fertile lherzolite xenoliths. The bimodal xenolith suites are located above a recently detected low-velocity anomaly in the underlying upper mantle (Frederiksen AW, Bostock MG, Van Decar JC, Cassidy J, submitted to Tectonophysics). Two possible explanations for the correlation of the bimodal xenolith suites with the underlying zone of anomalously hot mantle are:

1. The harzburgite xenoliths may represent actual fragments of the anomalously hot asthenospheric mantle, while the lherzolite xenoliths represent the regional lithospheric upper mantle.
2. Both harzburgite and lherzolite xenoliths represent samples of the lithospheric mantle, but the harzburgite xenoliths represent lower lithosphere that has melted due to the influence of the underlying anomalously hot mantle.

This paper examines these two possibilities using both major and trace element data from seven mantle xenolith suites in the northern Canadian Cordillera. We argue that the harzburgite xenoliths of the bimodal suites reflect the partial melting of the lower lithosphere in response to the rise of fluids and heat from anomalously hot mantle below.

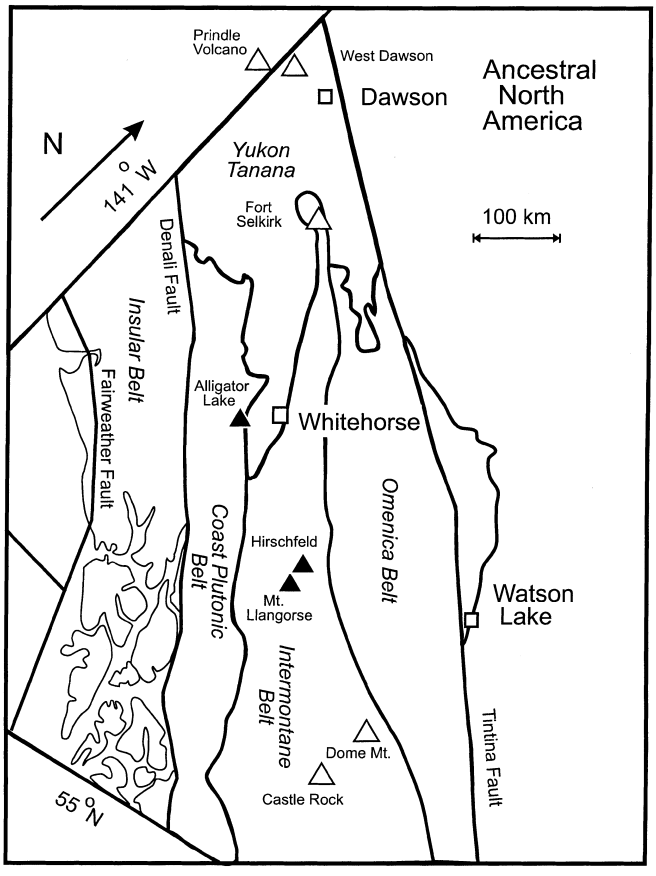

Fig. 1 Map showing major terrains and xenolith suites. (*Black triangles* bimodal suites, *open triangles* unimodal suites)

Locations and petrography

Numerous mid-Tertiary to Quaternary alkaline volcanic complexes occur along the northern Canadian Cordillera and a significant number contain abundant peridotite xenoliths and xenocrysts. In addition to our existing collections of mantle xenoliths from Alligator Lake, Fort Selkirk, Castle Rock, and Prindle Volcano (Prescott 1983; Francis 1987), we have sampled four newly discovered mantle xenolith suites at Mt. Llangorse, Hirschfeld Creek, and Dome Mt. in northern B.C. and West Dawson in Yukon (Fig. 1).

The petrography and mineral chemistry of the xenoliths from Fort Selkirk, Castle Rock, and Prindle Volcano were studied by Prescott (1983). The petrography and major element compositions (Francis 1987), and isotopic characteristics (Carignan et al. 1996) of the Alligator Lake xenoliths have been previously published. The xenoliths are dominantly four-phase peridotites corresponding to the type I xenoliths of Frey and Prinz (1978) with olivine Fo contents ranging from 0.85 to 0.92. Most are spinel peridotites, although there are some plagioclase peridotites at Prindle Volcano and Castle Rock. Al-augite series or type II xenoliths and composite xenoliths are rare. The xenoliths are "dry" peridotites without hydrous minerals such as amphibole and mica, or melt pockets produced by the breakdown of hydrous minerals. Rare amphibole xenocrysts, however, have been observed at some of the xenolith localities.

The Cordilleran xenoliths have protogranular to porphyroclastic textures and most display textures transitional between these two, with both kinked porphyroclasts of olivine and enstatite and smaller neoblasts of all mineral phases. The lherzolite xenoliths from most suites are relatively fine grained (1–2 mm), except Fort Selkirk where the xenoliths are significantly coarser grained (>3 mm). In contrast, the harzburgite xenoliths in all suites tend to be slightly coarser grained (2–3 mm) than their associated lherzolite xenoliths. The lherzolite xenoliths display little or no foliation, while the harzburgite xenoliths exhibit a distinct foliation. No spinel-pyroxene symplectite textures are observed and there appears to be no preferential association between spinel and Cpx. The density of fluid inclusions in most of these xenoliths is relatively low (Nadeau et al. 1990).

The proportions of minerals in the Cordilleran xenoliths were estimated by a least square calculation in which the bulk rock composition was reproduced using the microprobe analyses of the mineral compositions. The xenoliths range from relatively pyroxene rich spinel lherzolite to olivine-rich harzburgite. Among the seven xenolith suites, three display bimodal xenolith populations consisting of both fertile lherzolite and refractory harzburgite, while the remaining four exhibit unimodal xenolith populations dominated by fertile lherzolites (Fig. 2). The lherzolite mode is centred at 13–15 wt% Cpx, while the harzburgite mode occurs at 2 wt% Cpx. Most harzburgite xenoliths have Cpx contents lower than average abyssal harzburgites (Johnson et al. 1990), but similar to harzburgite xenoliths from the Islands of Savai'i and Tubuai in the south Pacific (Hauri and Hart 1994).

The three bimodal xenolith suites are located near the B.C.–Yukon border, the Alligator Lake suite within the Coast Plutonic belt of the southern Yukon and the Mt. Llangorse and Hirschfeld Creek suites within the intermontane belt of northern British Colombia. Their location appears to be correlated with a P-wave slowness anomaly detected teleseismically (Frederiksen AW, Bostock MG, Van Decar JC, Cassidy J, submitted to Tectonophysics) in the mantle beneath the southern Yukon (Fig. 3). This region of anomalously slow mantle has a diameter of about 200 km and extends from the base of the lithosphere down to depths of 400–

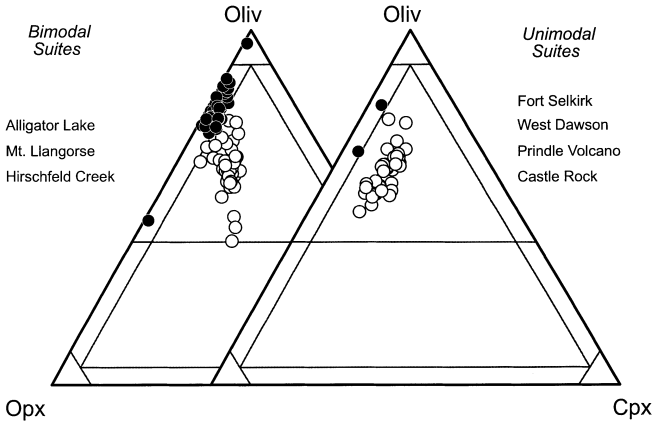

Fig. 2 Modal proportions of xenoliths in bimodal and unimodal suites. (*Black circles* harzburgites, *open circles* lherzolites)

500 km. The 3% magnitude of the seismic anomaly appears to require a temperature anomaly on the order of 200 °C hotter than the surrounding mantle, if no interstitial melt is present. Frederiksen argued that the mantle anomaly resulted from asthenosphere upwelling related to a slab window under the northern Cordillera. They proposed that the retreat of the slab decompressed the underlying asthenosphere and brought hotter material from depth into the slab window.

Analytical techniques

The major element compositions of bulk xenoliths were determined with a Philips PW1400 X-ray fluorescence spectrometer on powders made from 50–200 cm^3 cut blocks, and the major element compositions of all mineral phases were determined with a JEOL 8900 super microprobe, both at McGill University. Trace elements in Cpx grains were analysed in situ with a Fisions-VG Nd:YAG (1064 nm) laser and Fisions-VG PQII + ICP-MS (LAM-ICP-MS) at the Université de Montréal. The Cpx grains for trace element analysis were hand-picked with a binocular microscope in order to obtain inclusion-free grains. The picked grains were washed in an ultrasonic bath with distilled water for 20 minutes and mounted in plastic blocks with epoxy. The analyses were performed in Q-switched mode at a repetition rate of 5 and a flashlamp voltage of 630 volts, which resulted in a beam size of about 80 μm. The trace elements were divided into two menus that were analysed in separate runs in order to obtain sufficiently long measurement times before the laser beam penetrated the samples. Data were collected in peak jumping mode with three channels for each peak. A dwell time of 10 μs was used for each element such that, for a total acquisition time of 60 seconds, each element was counted for a total of more than 1 second. Prior to each analysis, the spot was pre-ablated for 20 seconds to eliminate surface effects and obtain a stable signal. The major element Ca (determined by electron microprobe) was used as internal standard to eliminate ablation yield effects. Spiked silicate reference glass NIST-612 (doped with 40 trace elements at levels of about 40 ppm) was used as a calibration standard. Precision and accuracy were estimated by repeat analysis of reference standards of augite and amphibole xenocrysts from Kakanui, New Zealand, whose trace element compositions were determined by ICP-MS in solution mode at the University of Memorial. For most elements with concentrations greater than 1 ppm, both precision and accuracy were better than 5% (Table 1). The accuracy of the LAM-ICP-MS analyses was checked by cross calibration with the Cameca IMS 3f ion microprobe at Woods Hole Oceanographic Institution. A comparison of the results indicates that the agreement between these two techniques is excellent (Fig. 4), despite the much larger volume sampled by the laser (Fig. 5). The Ti contents in the Cpx of some harzburgite xenoliths are lower than the detection limit (250 ppm) of the electron microprobe (Roden and Shimizu 1993). In such cases, the LAM-ICP-MS value for Ti is presented in place of electron microprobe values. Tests for trace element zoning indicated that the Cpx of most xenoliths were homogeneous, and the values reported in this work represent the average of four analyses, two spots on one grain, and one spot on each of two other grains.

Fig. 3a, b Teleseismic images of the upper mantle beneath the northern Cordillera with the locations of the xenolith suites superimposed: **a** 200 km plan; **b** section D–D'. *Symbols* as in Fig. 1

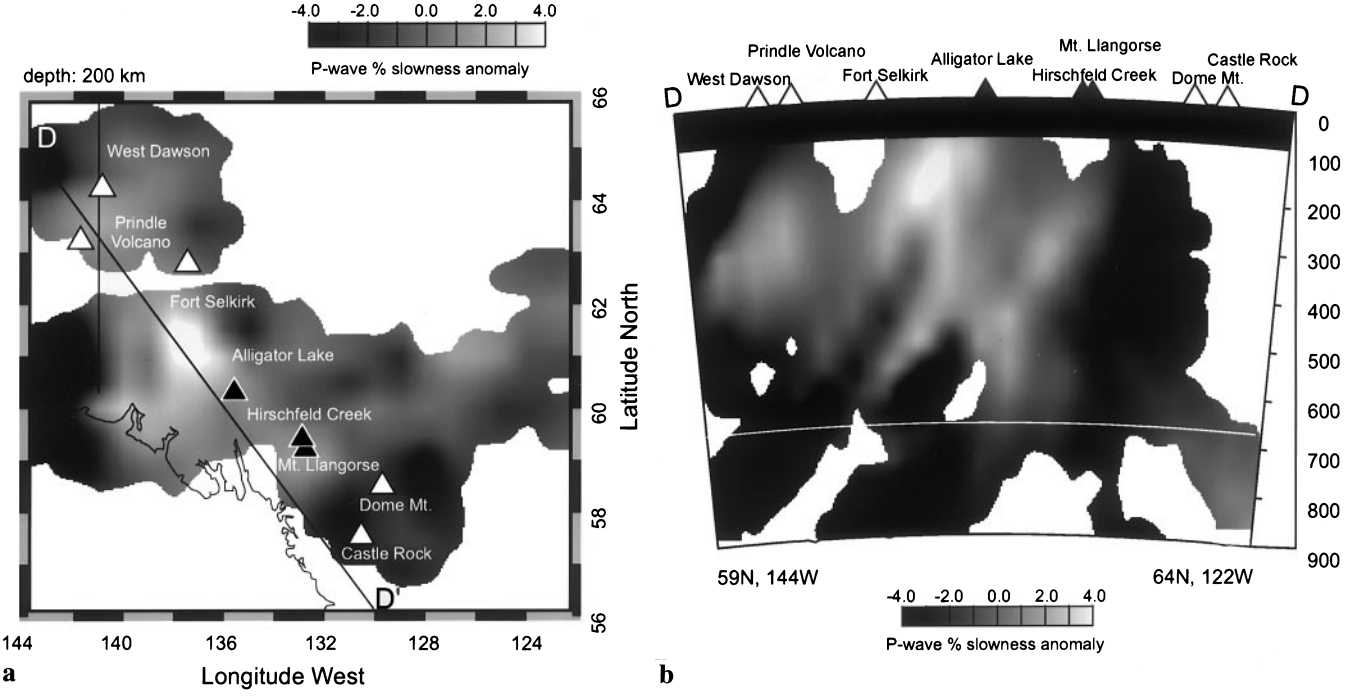

Table 1 Analyses of amphibole and augite megacrysts from Kakanui, New Zealand. Solution-ICP-MS analysis of internal standards for LAM-ICP-MS analysis performed at Memorial University. [*n* and the *numbers inside brackets* represent the number of analyses, *SD* represents standard deviation (1σ)]

	Amphibole		Augite	
	Major element analyses			
	Wt% $n = 40$	SD	Wt% $n = 30$	SD
SiO_2	39.70	0.14	49.37	0.25
TiO_2	24.90	0.05	1.12	0.08
Al_2O_3	13.84	0.08	8.83	0.10
FeO	12.19	0.17	6.83	0.14
MgO	12.05	0.09	14.98	0.10
MnO	0.12	0.03	0.13	0.03
CaO	9.91	0.10	16.68	0.17
K_2O	2.08	0.03	0.02	0.02
Na_2O	2.77	0.05	1.50	0.02
Cr_2O_3			0.01	0.01
NiO			0.03	0.02
Total	97.57	0.27	99.50	0.28

	Trace element analyses (in ppm)					
	Laser $n = 75$	SD	Solution (ICP-MS) $n = 2$	Laser $n = 38$	SD	Solution (ICP-MS) $n = 2$
Sc	21	1		39	1	
Ti	3573	43		887	8	
V	344	8		325	12	
Rb	15(2)	0	15			
Sr	489	17	497	74	1	73
Ba	253(2)	0	254			22
Th	0.04	0.01	0.06			0.07
Y	8.1	0.3	9.0	9.4	0.3	9.5
Zr	58	2	69	31	1	33
Nb	27	1	28	0.36	0.03	0.42
Hf	2.6	0.1	2.9	1.1	0.1	1.6
La	5.1	0.3	5.3	2.0	0.1	2.3
Ce	17	1	18	7.9	0.2	12
Pr	3.1	0.2	3.2	1.5	0.1	1.5
Nd	16	1	16	8.4	0.2	8.4
Sm	4.5	0.2	4.5	2.7	0.2	2.7
Eu	1.6	0.1	1.6	1.0	0.1	1.0
Gd	3.7	0.0	4.5	0.44	0.02	0.44
Tb	0.51	0.21	0.53	3.0	0.2	3.0
Dy	2.5	0.2	2.7	2.5	0.1	2.5
Ho	0.37	0.03	0.39	0.41	0.03	0.41
Er	0.71	0.07	0.79	0.93	0.07	0.95
Tm	0.07	0.01	0.08	0.11	0.00	0.11
Yb	0.30	0.04	0.32	0.55	0.06	0.54
Lu	0.02	0.01	0.03	0.06	0.01	0.05

Results

Major element compositions

The major element compositions of more than 200 xenoliths were analysed in order to determine the compositional populations of the different mantle xenolith suites (Table 2). The two types of xenolith population are clearly visible in the major element compositions of the xenoliths (Fig. 6). The xenoliths from the bimodal suites display two compositional clusters that are separated by a distinct population minimum. One cluster consists of Al-poor harzburgite xenoliths, while the other cluster is comprised of fertile lherzolites with similar Al contents to those of the lherzolites of the unimodal suites. The lherzolites have higher Al_2O_3, CaO, TiO_2, and SiO_2, but lower MgO and NiO than the harzburgite xenoliths. The most fertile lherzolite xenoliths (AL-46, LG-36N) have major element compositions close to that of pyrolite (Ringwood 1975). Despite the compositional discontinuity between the lherzolite and harzburgite xenoliths, taken as a whole, the major element compositions of the Cordilleran xenoliths display a systematic variation in which MgO is negatively correlated with Al_2O_3, CaO, TiO_2, SiO_2, FeO, and Na_2O, and positively correlated with NiO (Fig. 7). There is little or no variation in

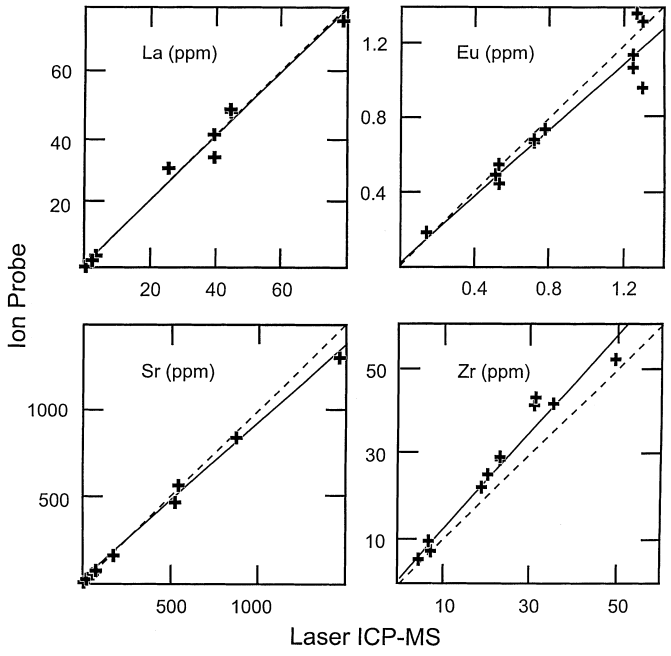

Fig. 4 Comparison of trace element analyses of Cpx by LAM-ICP-MS and ion probe techniques. *Solid lines* represent regression lines; *dashed lines* represent 1:1 correspondence

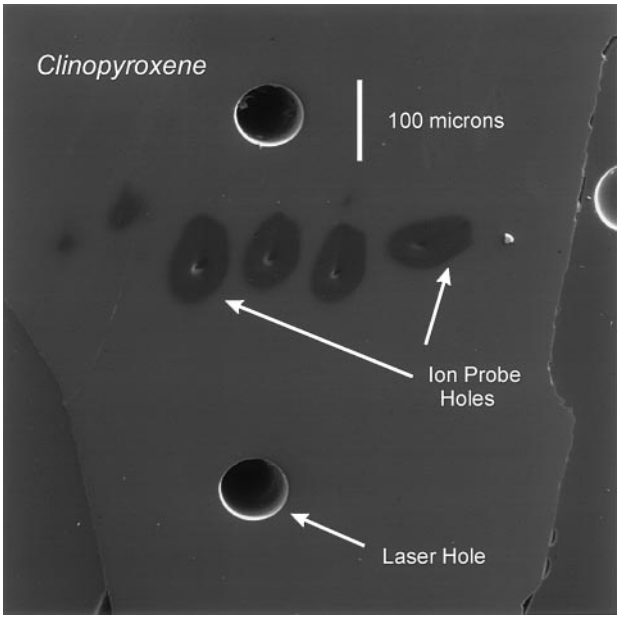

Fig. 5 Laser ablation and ion probe sampling holes

Cr_2O_3 with MgO. Similar major element variations have been observed in mantle xenoliths hosted by alkali basalts around the world (Maaløe and Aoki 1977) and in the residues of melting experiments on model mantle peridotites (Mysen and Kushiro 1977; Jaques and Green 1980).

There are systematic variations in the compositions of the xenolith minerals (Tables 3–6) and a distinct compositional gap between the mineral phases of the

Table 2 Representative analyses of bulk xenoliths (wt%). X-Ray fluorescence analyses of bulk rocks were performed by Tariq Ahmadali at McGill University. The analytical technique and the precisions have been previously described (Francis 1987). (Labels: *LG* Mt. Llangorse, *HF* Hirschfeld Creek, *FS* Fort Selkirk, *WD* West Dawson, *PV* Prindle Volcano, *CR* Castle Rock.) Bulk rock analyses of Alligator Lake xenoliths can be found in Francis, 1987

Sample	LG-36	LG-4	LG-12	HF-24	HF-23	HF-7	FS-10	FS-45	WD-12	WD-17	PV-4	CR-33
Rock type	Lherzolite	Harzburgite	Harzburgite	Lherzolite	Harzburgite	Harzburgite	Lherzolite	Harzburgite	Lherzolite	Lherzolite	Lherzolite	Lherzolite
SiO_2	44.58	43.32	43.28	44.22	43.90	43.64	44.73	42.83	43.92	43.86	44.84	44.48
TiO_2	0.07	0.01	0.00	0.07	0.01	0.03	0.13	0.08	0.06	0.06	0.13	0.09
Al_2O_3	3.46	0.60	0.74	3.20	1.40	1.03	3.86	2.44	2.71	2.66	3.91	3.02
Cr_2O_3	0.40	0.32	0.46	0.38	0.41	0.41	0.46	0.53	0.45	0.34	0.40	0.43
MgO	38.90	46.91	46.73	39.62	44.77	45.60	37.66	39.85	41.31	41.31	38.41	40.11
FeO	8.04	7.92	7.93	8.78	7.81	8.18	8.32	9.05	8.03	8.80	8.32	8.46
MnO	0.13	0.13	0.12	0.14	0.12	0.13	0.14	0.15	0.13	0.14	0.14	0.14
CaO	2.96	0.54	0.53	2.92	1.10	0.75	3.29	2.71	2.34	2.63	3.45	2.55
NiO	0.28	0.35	0.35	0.28	0.34	0.34	0.26	0.28	0.29	0.30	0.27	0.30
Na_2O	0.16	0.00	0.00	0.18	0.03	0.00	0.29	0.57	0.18	0.06	0.23	0.21
K_2O	0.01	0.01	0.01	0.01	0.08	0.02	0.01	0.26	0.01	0.01	0.02	0.01
P_2O_3	0.02	0.01	0.00	0.00	0.01	0.02	0.01	0.35	0.01	0.00	0.01	0.00
Loss on ignition	0.01	0.00	0.00	0.00	0.00	0.00	0.00	0.00	0.00	0.00	0.00	0.00
Total	99.03	100.12	100.16	99.80	99.98	100.14	99.16	99.09	99.43	100.17	100.12	99.79

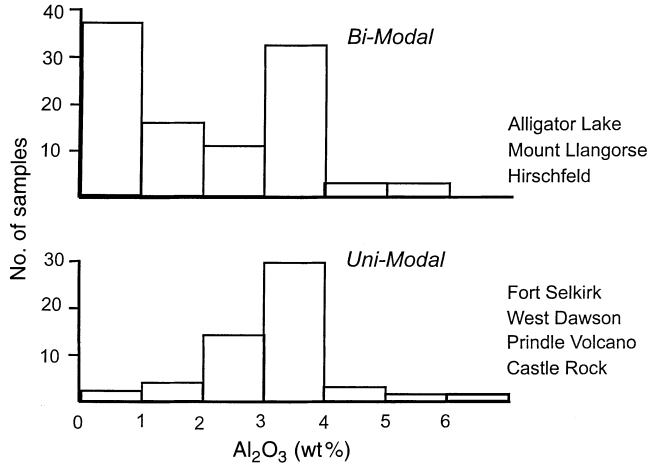

Fig. 6 Histogram of Al content (wt%) of xenoliths from bimodal and unimodal xenolith suites

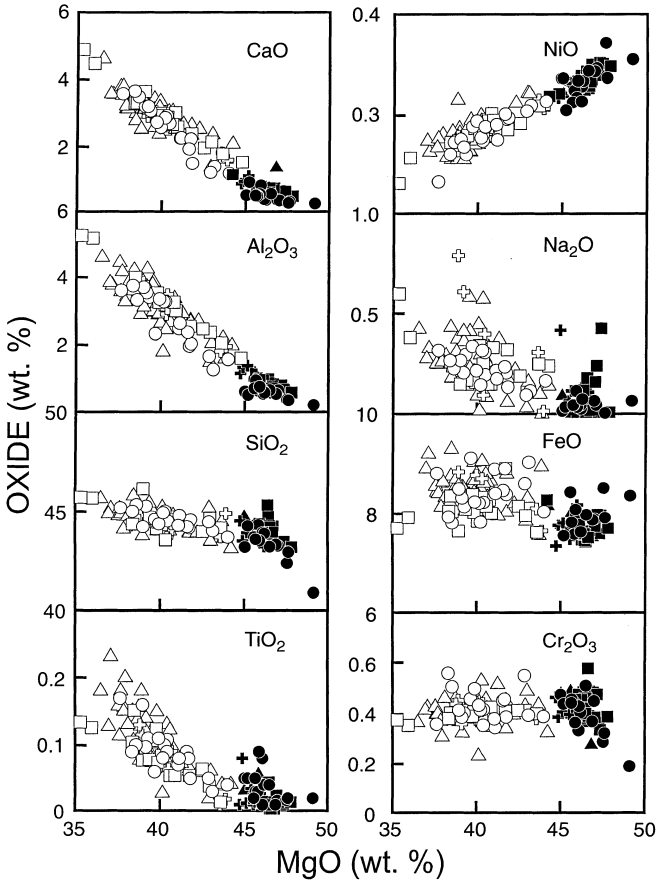

Fig. 7 Variation of major oxides with MgO for Cordillera xenoliths. (Symbols: *black symbols* harzburgites, *open symbols* lherzolites, *circles* xenoliths from Alligator Lake, *squares* from Mt. Llangorse, *crosses* from Hirschfeld Creek, *triangles* xenoliths in unimodal suites)

harzburgite and lherzolite xenoliths. The harzburgite xenoliths are characterised by higher olivine Fo contents and spinel Cr# [Cr / (Cr + Al)] values, but lower Cpx Al contents than the lherzolite xenoliths (Fig. 8). The

Table 3 Representative analyses of olivines (wt%). The microprobe analyses of all mineral phases were performed with JEOL 8900 super probe at McGill University using WDS mode, 20 Kv acceleration voltage, 20 nA beam current, and 5 μm beam size. Counting times of 30 s were used for most elements, but 100 s counting times were used for Ti and Ca in Cpx, because the former is low in harzburgite Cpx and the latter was used as an internal standard for trace element analysis by LAM-ICP-MS. The listed data represent the averages of four analyses. *Labels* as in Table 2. Microprobe analyses of mineral phases in Alligator Lake xenoliths can be found in Francis, 1987

Sample	LG-36	LG-4	LG-12	HF-24	HF-23	HF-7	FS-10	FS-8	WD-12	WD-17	PV-4	CR-33
SiO_2	40.80	40.84	41.33	40.80	40.97	41.40	39.92	40.82	40.99	40.86	40.78	40.84
TiO_2	0.00	0.00	0.00	0.00	0.00	0.00	0.00	0.00	0.00	0.00	0.00	0.01
Al_2O_3	0.02	0.00	0.00	0.00	0.00	0.00	0.00	0.00	0.01	0.01	0.02	0.05
Cr_2O_3	0.00	0.01	0.03	0.00	0.01	0.01	0.00	0.01	0.00	0.01	0.00	0.03
MgO	48.72	49.63	50.11	48.59	49.86	49.95	49.22	50.83	49.28	48.72	48.47	48.75
FeO	9.67	8.05	8.30	10.42	8.39	8.50	10.58	8.34	9.24	9.78	9.97	9.44
MnO	0.13	0.11	0.12	0.15	0.12	0.13	0.13	0.10	0.12	0.14	0.14	0.13
CaO	0.03	0.07	0.05	0.03	0.02	0.03	0.06	0.04	0.05	0.05	0.03	0.14
NiO	0.31	0.30	0.31	0.30	0.33	0.31	0.36	0.39	0.30	0.31	0.30	0.29
Na_2O	0.02	0.00	0.00	0.01	0.00	0.00	0.00	0.00	0.00	0.00	0.00	0.02
K_2O	0.00	0.00	0.00	0.00	0.00	0.00	0.00	0.00	0.00	0.00	0.00	0.00
P_2O_5	0.00	0.00	0.00	0.00	0.00	0.00	0.00	0.00	0.00	0.00	0.00	0.00
Total	99.71	99.01	100.26	100.30	99.70	100.32	100.27	100.52	100.00	99.87	99.71	99.69

Table 4 Representative analyses of orthopyroxenes (wt%). The microprobe analyses of all mineral phases were performed with JEOL 8900 super probe at McGill University using WDS mode, 20 Kv acceleration voltage, 20 nA beam current, and 5 μm beam size. Counting times of 30 s were used for most elements, but 100 s counting times were used for Ti and Ca in Cpx, because the former is low in harzburgite Cpx and the latter was used as an internal standard for trace element analysis by LAM-ICP-MS. The listed data represent the averages of four analyses. *Labels* as in Table 2. Microprobe analyses of mineral phases in Alligator Lake xenoliths can be found in Francis, 1987

Sample	LG-36	LG-4	LG-12	HF-24	HF-23	HF-7	FS-10	FS-8	WD-12	WD-17	PV-4	CR-33
SiO_2	54.94	56.20	56.74	54.62	55.30	55.86	54.42	56.44	54.60	54.85	54.90	53.44
TiO_2	0.06	0.00	0.00	0.06	0.00	0.07	0.13	0.02	0.09	0.08	0.09	0.12
Al_2O_3	4.47	2.09	2.11	4.35	3.39	3.10	4.72	2.06	4.58	4.64	4.19	5.90
Cr_2O_3	0.31	0.52	0.50	0.31	0.60	0.52	0.35	0.54	0.45	0.38	0.24	0.57
MgO	33.33	34.61	34.96	33.30	34.33	34.54	32.68	34.79	33.36	33.20	33.22	31.82
FeO	6.34	5.31	5.26	6.89	5.61	5.62	6.63	5.11	5.94	6.40	6.68	6.10
MnO	0.12	0.13	0.11	0.16	0.12	0.14	0.17	0.13	0.15	0.15	0.14	0.14
CaO	0.54	0.65	0.70	0.56	0.61	0.69	0.55	0.69	0.78	0.78	0.57	1.46
NiO	0.09	0.09	0.09	0.05	0.09	0.06	0.00	0.00	0.06	0.08	0.11	0.11
Na_2O	0.06	0.05	0.02	0.04	0.04	0.01	0.06	0.02	0.09	0.05	0.05	0.18
K_2O	0.02	0.02	0.01	0.02	0.01	0.02	0.00	0.00	0.01	0.02	0.02	0.01
P_2O_5	0.00	0.00	0.00	0.00	0.00	0.00	0.00	0.00	0.00	0.00	0.00	0.00
Total	100.28	99.67	100.50	100.35	100.11	100.62	99.72	99.79	100.10	100.63	100.19	99.86

Table 5 Representative analyses of clinopyroxenes (wt%). The microprobe analyses of all mineral phases were performed with JEOL 8900 super probe at McGill University using WDS mode, 20 Kv acceleration voltage, 20 nA beam current, and 5 μm beam size. Counting times of 30 s were used for most elements, but 100 s counting times were used for Ti and Ca in Cpx, because the former is low in harzburgite Cpx and the latter was used as an internal standard for trace element analysis by LAM-ICP-MS. The listed data represent the averages of four analyses. *Labels* as in Table 2. Microprobe analyses of mineral phases in Alligator Lake xenoliths can be found in Francis, 1987

Sample	LG-36	LG-4	LG-12	HF-24	HF-23	HF-7	FS-10	FS-15	WD-12	WD-17	PV-4	CR-33
SiO_2	52.03	53.08	53.80	51.49	52.37	52.84	51.73	51.94	52.20	51.58	51.37	51.19
TiO_2	0.34	0.02	0.02	0.32	0.02	0.19	0.55	0.48	0.32	0.33	0.53	0.38
Al_2O_3	6.66	3.10	2.30	6.20	3.99	3.06	7.07	6.06	6.01	6.54	6.40	6.79
Cr_2O_3	0.77	1.47	0.89	0.74	1.13	0.81	0.72	0.83	0.92	0.80	0.61	0.84
MgO	14.96	16.86	17.79	15.22	16.49	17.36	14.59	15.15	15.73	15.83	15.04	16.78
FeO	2.71	2.05	2.00	2.85	2.17	2.08	2.62	2.46	2.70	2.87	2.89	3.35
MnO	0.10	0.09	0.08	0.09	0.07	0.08	0.09	0.07	0.07	0.11	0.10	0.09
CaO	20.67	21.48	22.99	21.16	22.18	23.24	20.39	21.27	20.68	21.21	21.25	18.92
NiO	0.07	0.05	0.02	0.04	0.04	0.06	0.02	0.00	0.06	0.08	0.04	0.05
Na_2O	1.78	1.18	0.41	1.43	0.98	0.39	1.82	1.38	1.50	1.19	1.45	1.26
K_2O	0.02	0.01	0.02	0.02	0.02	0.01	0.00	0.00	0.01	0.02	0.02	0.02
P_2O_5	0.01	0.05	0.04	0.04	0.05	0.03	0.06	0.00	0.03	0.08	0.07	0.03
Total	100.11	99.43	100.37	99.59	99.52	100.16	99.65	99.64	100.23	100.65	99.79	99.71

Table 6 Representative analyses of spinels (wt%). The microprobe analyses of all mineral phases were performed with JEOL 8900 super probe at McGill University using WDS mode, 20 Kv acceleration voltage, 20 nA beam current, and 5 μm beam size. Counting times of 30 s were used for most elements, but 100 s counting times were used for Ti and Ca in Cpx, because the former is low in harzburgite Cpx and the latter was used as an internal standard for trace element analysis by LAM-ICP-MS. The listed data represent the averages of four analyses. *Labels* as in Table 2. Microprobe analyses of mineral phases in Alligator Lake xenoliths can be found in Francis, 1987

Sample	LG-36	LG-4	LG-12	HF-24	HF-23	HF-7	FS-12	FS-8	WD-12	CR-18	PV-4	CR-8
SiO_2	0.01	0.00	0.00	0.00	0.00	0.00	0.08	0.03	0.01	0.00	0.00	0.06
TiO_2	0.04	0.02	0.00	0.07	0.01	0.14	0.14	0.06	0.11	0.08	0.08	0.15
Al_2O_3	59.01	30.27	31.04	58.61	44.84	42.21	59.91	57.23	54.40	57.02	59.16	54.89
Cr_2O_3	9.21	40.37	39.42	9.52	24.06	27.23	7.28	10.45	13.52	10.78	8.26	12.57
MgO	21.03	17.15	16.85	20.65	18.71	18.44	21.59	20.36	20.79	20.99	20.89	21.46
FeO	10.29	12.09	12.64	10.76	11.97	11.98	11.12	11.33	10.91	11.07	10.71	10.39
MnO	0.11	0.17	0.21	0.11	0.15	0.15	0.10	0.10	0.13	0.11	0.10	0.12
CaO	0.01	0.00	0.00	0.00	0.00	0.00	0.00	0.00	0.00	0.00	0.00	0.00
NiO	0.39	0.15	0.16	0.36	0.24	0.21	0.40	0.33	0.33	0.36	0.40	0.34
Na_2O	0.00	0.00	0.00	0.00	0.00	0.00	0.00	0.00	0.00	0.00	0.00	0.00
K_2O	0.00	0.00	0.00	0.00	0.00	0.00	0.00	0.00	0.00	0.00	0.00	0.00
P_2O_5	0.00	0.00	0.00	0.00	0.00	0.00	0.00	0.00	0.00	0.00	0.00	0.00
Total	100.09	100.23	100.33	100.07	99.97	100.37	100.63	99.90	100.21	100.43	99.61	99.98

olivine Fo contents (Fo = 0.90–0.92) in the harzburgite xenoliths are similar to those of extremely refractory harzburgite xenoliths from the Islands of Savai'i and Tubuai (Hauri and Hart 1994).

The equilibration temperatures of the xenoliths were calculated using Wells' two-pyroxene geothermometer (Wells 1977) that has been shown to reproduce more recent experiments around 900 °C (Brey and Köhler 1990) very well. The Opx-Ca geothermometer (Sachtleben and Seck 1981) yields slightly higher temperatures than that of Wells, but the range of calculated temperatures is similar and the calculated temperatures of the harzburgites by both thermometers are typically 60–80 °C higher than those of the lherzolites in each bimodal xenolith suite (Fig. 9). For example, the average equilibration temperature in the harzburgites from Alligator Lake is 1040 °C, as compared to 956 °C for the lherzolites of the same suite. The equilibration temperatures of all Alligator Lake xenoliths, however, are higher than those from all the other xenolith suites.

Trace elements in Cpx

Clinopyroxene (Cpx) is the main carrier of REE (rare earth elements) and Sr in dry spinel peridotites (Rampone et al. 1991; McDonough et al. 1992; Roden and Shimizu 1993) and therefore the Cpx contents of these trace elements are representative of the xenolith as a whole. Xenoliths covering the compositional range in each suite were selected for in situ LAM-ICP-MS analysis (Table 7). Trace element contents in individual Cpx grains within most xenoliths are homogeneous, although the Cpx in Castle Rock xenoliths appear to have heterogeneous trace element contents. There is a large variation in the levels of highly incompatible trace elements [e.g. L (light) REE, Sr], whereas the variation in compatible and moderately incompatible elements [e.g. Sc, V, H (heavy) REE] is more limited. The abundances of the latter correlate with the Al and Ti contents of both the bulk xenoliths and Cpx and are distinct in the harzburgite and lherzolite Cpx. For example, the Yb contents of Cpx in xenoliths from the bimodal suites fall into two distinct clusters. Harzburgite Cpx have Yb contents around 0.3 ppm, whereas Yb contents in lherzolite Cpx range from 1.2 to 2.1 ppm. The Cpx in the lherzolites of the unimodal suites display Yb variations similar to those of the lherzolites of the bimodal suites.

The Cpx in many of the Cordilleran xenoliths display enrichment in highly incompatible trace elements such as LREE, Sr, and Zr. Moreover, this enrichment is more intensive in bimodal xenolith suites, whose Cpx are typically LREE-enriched, in contrast to the LREE-depleted Cpx which dominates the xenoliths of unimodal suites. Within the bimodal suites, Cpx in harzburgite xenoliths exhibit much higher incompatible trace element contents than Cpx in lherzolite xenoliths. The Cpx in some harzburgite xenoliths (AL-41, AL-52) display

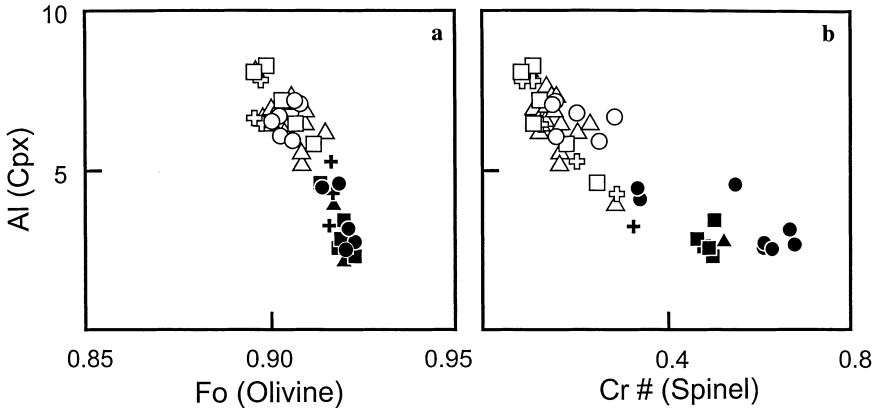

Fig. 8a, b Variations in composition of minerals in Cordilleran xenoliths. **a** Al (cation) in Cpx versus olivine Fo content. **b** Al (cation) in Cpx versus spinel Cr#. *Symbols* as in Fig. 7

LREE and Sr contents that are similar to the extreme values observed in the Cpx of harzburgites from the Islands of Savai'i, Tubuai, and Kerguelen (Hauri et al. 1993; Schiano et al. 1994). Overall, there is an inverse correlation between the ratios of Ce/Yb and Al content in the Cpx of the xenoliths from the bimodal suites (Fig. 10). Similar inverse correlations between major element fertility and highly incompatible trace elements have been reported in many xenoliths around the world (McDonough and Frey 1989).

In general, there are two different REE patterns in the Cpx of Cordilleran mantle xenoliths. The harzburgite Cpx exhibit REE patterns with steep negative slopes, while the lherzolite Cpx from all xenolith suites display REE patterns with variable and typically relatively low LREE contents, but flat MREE to HREE patterns (Fig. 11). All Cpx display Nb, Zr, Hf, and Ti depletions relative to REE of similar compatibility and, in general, the harzburgite Cpx exhibit greater HFSE depletions than the lherzolite Cpx. The highly incompatible trace elements in the Cpx of the bimodal suites appear to be correlated positively with pyroxene equilibration temperature (Fig. 12) and enrichment in $^{206}Pb/^{204}Pb$ (Fig. 13). In summary, the harzburgite xenoliths are the most depleted in major elements and mildly incompatible trace elements, but the most enriched in incompatible trace elements and have the most radiogenic Pb and Sr isotopic compositions, and have the highest equilibration temperatures.

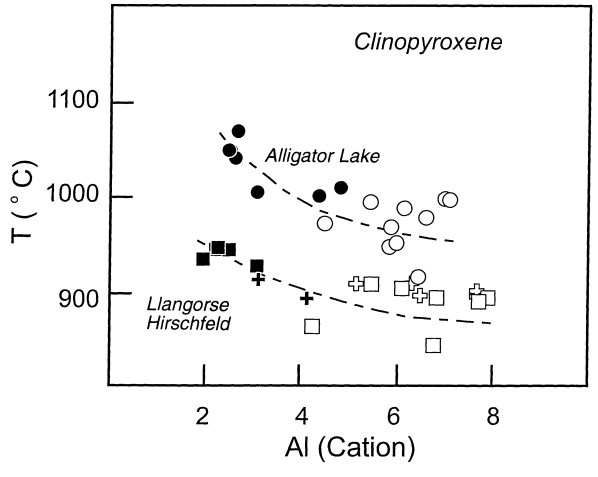

Fig. 9 Al (cation) of Cpx versus Wells' pyroxene temperature. Symbols as in Fig. 7. Harzburgites tend to have higher equilibration temperatures than lherzolites in all bimodal suites

Discussion

Although anomalously hot mantle has been detected beneath many recent volcanic regions (e.g. Granet et al. 1995; VanDecar et al. 1995; Wolfe et al. 1997), no correlations between the population of mantle xenoliths and the underlying anomalous mantle have been reported. The association of bimodal xenolith suites with the anomalous mantle beneath the southern Yukon suggests that these xenolith suites may either contain fragments of the anomalous mantle or that the lithospheric upper mantle has been affected by the anomalous mantle.

1. Evidence of a lithospheric mantle source

All the Cordilleran mantle xenoliths belong to the spinel lherzolite facies and thus come from depths between 30 and 80 km. Similar lherzolite xenoliths are present in both bimodal and unimodal suites and recent data on xenolith suites from the southern Cordillera (Peslier et al. 1997) indicate that they are also all dominated by fertile lherzolites. Furthermore, the lherzolites from all the Cordilleran suites have similar major element compositions and Cpx REE patterns, characterised by flat middle to HREE, but variable LREE. These REE patterns are similar to those of Cpx in mantle xenoliths from the Basin and Range province and Colorado Plateau of the western U.S. (Roden and Shimizu 1993) and from Hawaii (Sen et al. 1993). The absence of pyroxene-spinel intergrowths, along with the flat HREE patterns and the absence of positive Zr anomalies in lherzolite Cpx, argue against the lherzolites having originated in the garnet stability field (Shimizu 1975; Hauri and Hart 1994). This along with their dominance in all the unimodal suites

Table 7 Representative trace element analyses of clinopyroxenes (in ppm). Trace element compositions of clinopyroxenes were determined by LAM-ICP-MS. Analysis details in text. (*AL* Alligator Lake)

Sample	AL-47	AL-88	AL-41	AL-49	AL-52	AL-53	LG-30	LG-36	LG-4
Sc	85	79	83	90	85	68	85	88	125
Ti	2638	2038	98	5102	86	99	1439	2038	90
V	243	250	180	232	171	70	251	247	169
Th	0.3	0.2	5.0	4.2	3.1	3.4			1.8
Nb	0.7	0.3	2.0	0.6	1.1	0.9			2.7
Sr	25	26	1462.0	525	890	74	1.8	15	419
Zr	7.8	4.9	19	31	23	49	1.3	6.9	80
Y	15	14	3.8	4.2	3.1	5.7	14	16	7.2
Hf	0.7	0.4	0.2	0.4	0.1	1.2	0.2	0.5	0.4
La	1.6	1.2	79	40	59	45			21
Ce	2.6	1.1	162	60	92	73	0.05	0.30	58
Pr	0.35	0.18	16	5.7	9.8	7.8	0.03	0.14	7.2
Nd	1.9	1.7	51	23	36	28	0.47	1.5	29
Sm	1.5	1.0	5.2	4.3	5.7	3.7	0.47	1.95	5.1
Eu	0.48	0.51	1.3	1.3	1.3	1.3	0.28	0.49	1.5
Tb	0.40	0.41	0.31	0.32	0.29	0.36	0.29	0.40	0.41
Gd	2.0	2.2	2.7	3.0	2.9	2.8	1.5	2.1	3.0
Dy	2.8	2.9	1.3	1.2	1.0	1.6	2.5	2.9	1.8
Ho	0.63	0.65	0.19	0.19	0.12	0.26	0.58	0.68	0.30
Er	1.9	1.9	0.39	0.43	0.30	0.55	1.9	2.1	0.70
Tm	0.28	0.29	0.04	0.05	0.03	0.06	0.26	0.31	0.08
Yb	1.6	1.8	0.28	0.28	0.21	0.38	1.7	1.9	0.44
Lu	0.23	0.25	0.03	0.04	0.04	0.02	0.26	0.28	0.07
Sample	HF-2	HF-24	HF-7	FS-10	FS-15	WD-12	WD-14	PV-4	CR-33
Sc	81	89	76	75	78	72	76	93	84
Ti	2530	1912	1115	284	2878	1918	2018	3171	2302
V	245	245	166	287	271	268	287	241	216
Th			0.1			0.1	0.7		0.1
Nb	0.1	0.3	0.1	0.1		0.2	1.2	0.3	0.4
Sr	26	56	141	23	6.3	4.6	102	48	55
Zr	18	6.1	10	15	7.1	1.9	3.1	20	16
Y	18	17	7.5	17	16.8	13	13	19	15
Hf	0.8	0.4	0.3	0.7	0.6	0.2	0.3	1.0	0.7
La	0.18	1.4	1.2	0.10	0.02	0.49	4.7	0.60	1.0
Ce	1.2	2.9	5.8	1.2	0.27	0.35	9.5	2.2	1.7
Pr	0.32	0.38	1.3	0.38	0.19	0.05	0.66	0.57	0.34
Nd	2.6	1.9	7.4	2.7	1.7	0.69	3.1	3.8	2.2
Sm	1.5	1.0	1.9	2.0	1.5	0.71	1.0	1.7	1.2
Eu	0.64	0.44	0.60	0.61	0.53	0.38	0.45	0.76	0.49
Tb	0.48	0.36	0.26	0.48	0.47	0.34	0.37	0.53	0.40
Gd	2.5	1.9	1.8	2.7	2.4	1.7	1.9	2.9	1.9
Dy	3.3	2.8	1.7	3.5	2.9	2.6	2.3	3.7	2.6
Ho	0.78	0.63	0.31	0.76	0.73	0.62	0.54	0.75	0.55
Er	2.4	2.0	0.86	2.1	2.3	1.9	1.8	2.4	1.7
Tm	0.34	0.30	0.12	0.30	0.31	0.25	0.27	0.38	0.23
Yb	2.2	1.9	0.73	1.8	2.1	1.8	1.8	2.3	1.6
Lu	0.32	0.28	0.10	0.29	0.29	0.23	0.24	0.39	0.21

leads us to interpret the lherzolite xenoliths as samples of the regional lithospheric mantle beneath the Canadian Cordillera.

In contrast, harzburgite xenoliths are essentially restricted to the bimodal suites in the northern Cordillera. These harzburgites display distinct textures and major element and trace element compositions compared to the lherzolites. The harzburgite xenoliths tend to yield higher equilibration temperatures than associated lherzolite xenoliths (60–80 °C), suggesting that they may have been derived from about 8 km deeper than the lherzolite xenoliths, assuming the geotherm calculated for the Cordilleran upper mantle by Ranalli (1980). These differences suggest that the mantle sampled by the harzburgite xenoliths is physically separate from that sampled by the lherzolite xenoliths, and that harzburgite mantle may underlie a lherzolite lithospheric mantle. However, the lack of garnet in the harzburgites indicates that they are derived from shallower depths than the anomaly. Although the harzburgites might represent recrystallized samples of the underlying anomalous asthenospheric mantle, evidence linking the harzburgite and lherzolite xenoliths suggests that they also represent samples of the lithospheric mantle. First, the overall major element compositions of lherzolite and harzburgite xenoliths define a linear array which is

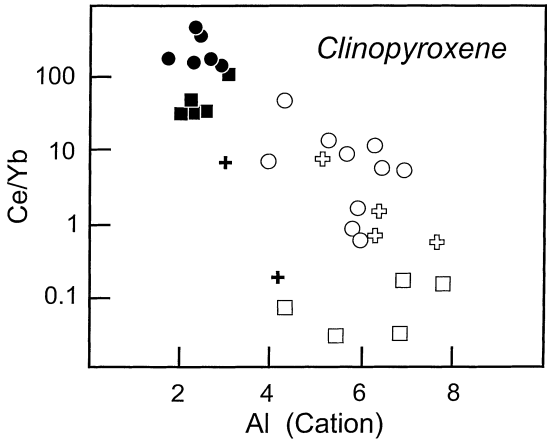

Fig. 10 Al (cation) versus Ce/Yb ratios for Cpx in bimodal suites. *Symbols* as in Fig. 7. The inverse correlation between Al and Ce/Yb ratios in Cpx is not consistent with closed system partial melting and reflects an incompatible trace element enrichment process

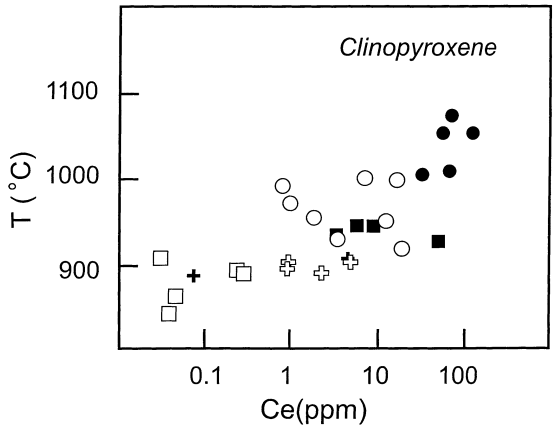

Fig. 12 Ce content of Cpx versus equilibration temperature (Wells 1977). Xenoliths with higher pyroxene temperatures have higher Ce contents. *Symbols* as in Fig. 7

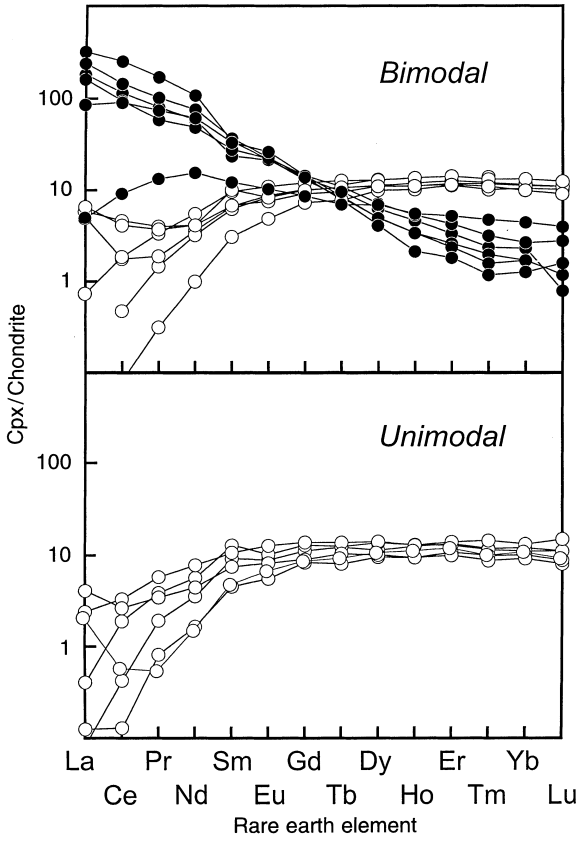

Fig. 11 Chondrite-normalised REE patterns for the Cpx from bimodal and unimodal suites. (*Black circles* harzburgite Cpx, *open circles* lherzolite Cpx)

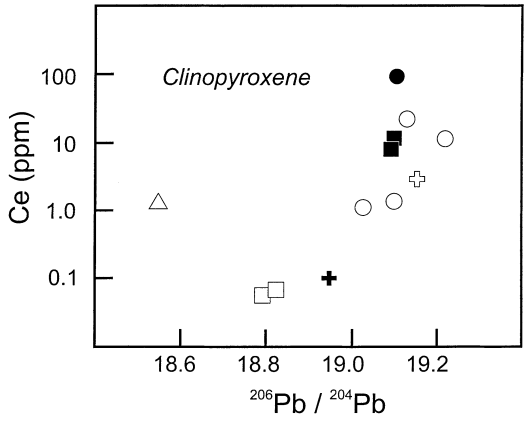

Fig. 13 Ce versus $^{206}Pb/^{204}Pb$ in Cpx. Pb isotopic data from Carignan et al. (1996). *Symbols* as in Fig. 7

consistent with the compositional trends of the residues of experimental melting of fertile mantle xenoliths (Mysen and Kushiro 1977; Jaques and Green 1980). The major element spectrum from fertile lherzolite to refractory harzburgite at Alligator Lake has been calculated to represent approximately 22% partial melting on the basis of mass balance and Fe/Mg partitioning between olivine and melt (Francis 1987). The HREE, Y, and Ti follow the major element variation and model calculations based on Yb and Ti contents of Cpx in the xenoliths indicate an average of 25% fractional melting (Fig. 14). The calculated extracted melts are Fe-poor, Si-rich picritic magmas whose compositions are similar to the late-Cretaceous (70 Ma) Carmacks volcanics in this region (Johnston et al. 1996). The compositional spectrum of the xenoliths in the Mt. Llangorse and Hirschfeld Creek suites can also be produced by similar extents of model partial melting. In addition, new Os isotopic data reveal that the harzburgites from the bimodal suites which are depleted in Al have the same $^{187}Os/^{186}Os$ as the prevalent lherzolite mantle, suggesting a genetic relationship between the harzburgite and lherzolite (Peslier et al. 1997).

Considering the large degree of melting required for the formation of the harzburgites, it might be argued that it is not surprising that no evidence of previous garnet remains. However, the persistence of spinel-py-

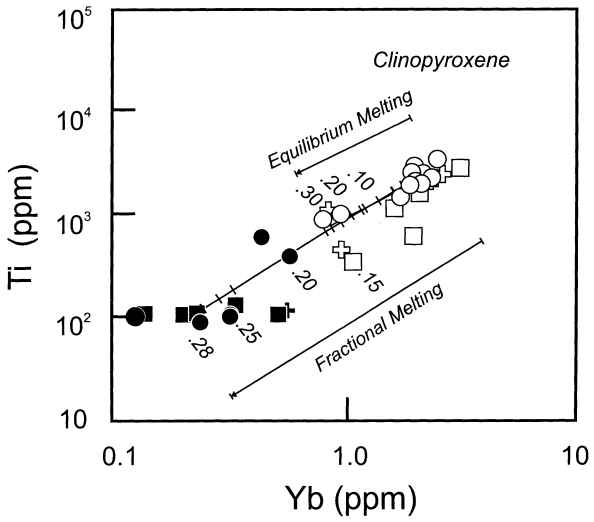

Fig. 14 Ti versus Yb for Cpx in bimodal xenolith suites, showing calculated trends for equilibrium and fractional melting using the method of Johnson et al. (1990). AL-46, whose composition is close to that of primitive mantle, was used as starting material with an initial mode of: Olivine (0.55), Opx (0.25), Cpx (0.18), Spinel (0.02), and a melt mode of: Olivine (0.10), Opx (0.20), Cpx (0.68), Spinel (0.02). *Numbers* indicate the extent of partial melting. *Symbols* as in Fig. 7.

roxene symplectities and Cpx with the trace element signature of garnet in harzburgite xenoliths from Savai'i that have experienced 33–45% melting (Hauri and Hart 1994) argues against the former presence of garnet in the Cordilleran harzburgite xenoliths.

2. Compositional and temperature influence on P-wave velocity

The relative P-wave velocity difference between the anomalous mantle underlying the bimodal suites and the surrounding mantle is about 3% (Frederiksen AW, Bostock MG, Van Decar JC, Cassidy J, submitted to Tectonophysics). Velocity perturbations in the upper mantle can be attributed to chemical composition, temperature, and the presence of an interstitial melt. In order to determine the effect of composition on velocity, we calculated the velocity difference between the most fertile lherzolite and the most refractory harzburgite at a depth within the garnet stability field using mineral modes calculated from their bulk composition and the available velocity data for individual minerals (Jordan 1979). We calculate a relative 0.8% velocity difference at a depth of 80 km, with the harzburgites being faster, not slower, than the lherzolites. The P-wave velocity has been shown to be most sensitive to the bulk Fe/(Fe + Mg) and the molar proportion of garnet (Jordan 1979). Increasing the garnet content of a rock increases P-wave velocity, whereas increasing the iron content decreases P-wave velocity. However, bulk Fe/(Fe + Mg) has a larger effect than garnet content and the higher Fe/(Fe + Mg) in the fertile lherzolite xenoliths results in lower velocities than the harzburgite xenoliths. Therefore, the compositional difference between the fertile lherzolite and refractory harzburgite xenoliths cannot produce the velocity differences detected teleseismically.

If we assume that the observed 3% velocity anomaly is a reflection of temperature difference, then the difference required is on the order of 600 °C using a temperature derivative for velocity of 0.5×10^{-5} K^{-1} (Anderson and Bass 1984). The inclusion of an anelasticity factor (Karato 1993) reduces the temperature difference to approximately 200 °C. Whichever temperature derivative is used, the anomalous mantle is at least 200 °C hotter than that of the surrounding mantle. This temperature difference is significantly greater than the maximum difference in pyroxene-equilibration temperature calculated for the lherzolites and harzburgites (60–80 °C), however the presence of interstitial melt in the asthenosphere would significantly reduce the required temperature difference.

3. Relation between the bimodal suites and the anomalous mantle

If neither the lherzolite nor harzburgite xenoliths are samples of the anomalous asthenospheric mantle, then the restriction of the harzburgite xenoliths to the bimodal suites, and their higher temperatures, suggest that the melting they have experienced may have been induced by the underlying anomalously hot mantle. Although it has been shown that conductive heating is unlikely to be responsible for significant degrees of partial melting of dry lithospheric peridotite (Arndt and Christensen 1992; Arndt et al. 1993), a number of workers have argued that melting of the lithosphere by conductive heating may be greatly facilitated if volatiles are involved (Hawkesworth et al. 1990; Gallagher and Hawkesworth 1992; Turner et al. 1996). Experimental studies have shown that the addition of as little as 0.3 wt% water will lower the solidus of peridotite by several hundred degrees and strongly increases the degree of melting at any given temperature (Olafsson and Eggler 1983; Hirose 1997). The extreme incompatible trace element abundances in the harzburgite Cpx suggest that the melting these harzburgite xenoliths have experienced was associated with an ingress of volatiles.

Constraints on the nature of the fluids involved during melting and metasomatism can be estimated from the trace element signature of the harzburgite Cpx. The calculated trace element characteristics of melts that would be in equilibrium with the harzburgite Cpx ($Kd^{cpx/melt}$, Hart and Dunn 1993; Green et al. 1992) define two end-members, one with extremely high Ce/Zr and Sr/Zr ratios but low Zr contents, similar to carbonatite melts, and the other with relatively lower trace element contents, similar to those expected for a residual liquid of the host alkaline basalt (Fig. 15). If the metasomatic agent were a water-rich fluid rather than a melt, then the partitioning coefficients of Brenan et al. (1995) indicate that its Sr/Th ratio was much higher than that

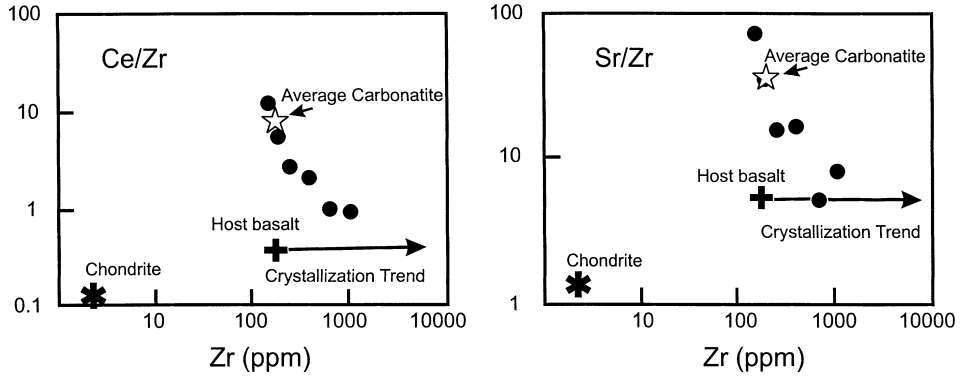

Fig. 15 Ce/Zr and Sr/Zr versus Zr in metasomatic fluids/melts calculated from trace element contents in highly enriched harzburgite Cpx and $kd^{cpx/melt}$ (Hart and Dunn 1993; Green et al. 1992). Average carbonatite from Wooley and Kempe (1989). The *arrow* indicates the trend expected for 97% fractional crystallisation of host alkaline basalt. $Kd^{cpx/melt}$ for Ce and Zr from Hart and Dunn (1993), $Kd^{amp/melt}$ for Ce from median value of Irving and Frey (1984), Kd for Zr from Adam et al. (1993)

of either carbonatite melts (Woolley and Kempe 1989) or the expected residual liquids of the host alkaline basalt.

The fact that the harzburgite xenoliths tend to have both higher incompatible trace elements and pyroxene equilibration temperatures suggests that the melting and enrichment processes were simultaneous. Although incompatible trace element enrichment has been observed in many mantle xenolith suites, enriched xenoliths do not typically display enhanced equilibration temperatures, and some even yield lower equilibration temperatures than associated xenoliths without incompatible trace element enrichment (Chen et al. 1989). Hauri and Hart (1994) found that two-pyroxene temperatures show a systematic increase with degree of LREE enrichment in Savai'i peridotites and interpreted this trend to result from magma-mantle interaction as proposed by Kelemen et al. (1992). In the model of Kelemen et al. (1992), however, the dissolution of Cpx transfers incompatible trace elements to the fluid, and the residual Cpx of the harzburgite has lower incompatible trace element contents than the Cpx of the original lherzolite (Kelemen et al. 1992; Takazawa et al. 1994). In contrast, the Cpx of the Cordilleran harzburgites have higher incompatible trace element contents than the lherzolite Cpx. In our model, the fluids or melts from the underlying anomalous mantle lowered the solidus of lherzolite lithosphere, causing melting, while at the same time leaving their enriched trace element signatures in the refractory harzburgite restite. This process was most intensive under Alligator Lake, whose harzburgites are both more depleted in fusible major elements and more enriched in highly incompatible trace elements than those of the Mt. Llangorse and Hirschfeld Creek suites. According to our model, this reflects the fact that the Alligator Lake suite is closer to the centre of the underlying anomalous mantle. Carignan et al. (1996) found that the Pb and Sr isotopic compositions of Cpx in the most enriched Alligator Lake xenoliths are similar to those of marine sediments in the northeastern Pacific and approach those of the enriched mantle end-member, EMII (Zindler and Hart 1986). They concluded that the enrichment of incompatible trace elements and Pb, Sr isotopes in the lithospheric mantle was related to subduction processes along the northern American continental margin. The U-Pb systematics of the metasomatic enrichment suggests that it is relatively recent (< 30 Ma, Carignan et al. 1996). However, the lack of a clear Pb isochron permits a large uncertainty in this estimate, and it is possible that the melting and metasomatism experienced by the harzburgites was associated with either the late Cretaceous (70 Ma) Carmacks volcanism or the Eocene magmatism that emplaced the granitoids of the Coast Plutonic Belt.

Concluding remarks

There are both bimodal and unimodal mantle xenolith suites in the Tertiary to Recent alkaline volcanic centres along the northern Canadian Cordillera. The unimodal suites are dominated by spinel lherzolite xenoliths and occur at many localities along the entire length of the Cordillera. The lherzolite xenoliths are thought to be samples of the prevalent upper mantle beneath the Cordillera. Three bimodal suites contain both fertile lherzolites and refractory harzburgites and are found above a region of anomalously hot asthenospheric mantle extending to depths of 400–500 km beneath the southwestern Yukon. The lherzolites of the bimodal suites are equivalent to those of the unimodal suites. The refractory harzburgites appear to be samples of partially melted lithospheric mantle. The evidence to date suggests that the harzburgites formed by approximately 20–25% partial melting of lherzolite lithosphere in response to the rise of fluids and heat from an underlying region of anomalously hot asthenospheric mantle.

Acknowledgements This research was supported by NSERC and LITHOPROBE grants to Don Francis and John Ludden. We would like to thank Tariq Ahmedali who performed the bulk xenolith XRF analyses and G. Gauthier and G. Poirier for their

help in obtaining the LAM-ICP-MS and electron microprobe results respectively. We also thank Dr. N. Shimizu of Woods Hole for his help in obtaining the ion-probe analyses that made possible the cross calibration of our LAM-ICP-MS data. The manuscript has benefited from reviews by M. Roden and C. Hawkesworth.

References

Adam J, Green TH, Sie SH (1993) Proton microprobe determined partitioning of Rb, Sr, Ba, Y, Zr, Nb, and Ta between experimentally produced amphiboles and silicate melts with variable F content. Chem Geol 109: 29–49

Anderson DL, Bass JD (1984) Mineralogy and composition of the upper mantle. Geophys Res Lett 11: 637–640

Arndt NT, Christensen U (1992) The role of lithospheric mantle in continental flood volcanism: thermal and geochemical constraints. J Geophys Res 97: 10967–10981

Arndt NT, Czamanske GK, Wooden JL, Fedorenko VA (1993) Mantle and crustal contributions to continental floor volcanism. Tectonophysics 223: 39–52

Brenan JM, Shaw HF, Ryerson FJ, Phinney DL (1995) Mineral-aqueous fluid partitioning of trace elements at 900 °C and 2.0 Gpa: constraints on the trace element chemistry of mantle and deep crustal fluids. Geochim Cosmochim Acta 59: 3331–3350

Brey GP, Köhler T (1990) Geothermobarometry in four-phase lherzolites. II. New thermobarometers, and practical assessment of existing thermobarometers. J Petrol 31: 1353–1378

Carignan J, Ludden J, Francis D (1996) On the recent enrichment of a subcontinental lithosphere: a detailed U-Pb study of spinel lherzolite xenoliths, Yukon, Canada. Geochim Cosmochim Acta 60: 4241–4252

Chen CY, Frey FA, Song Y (1989) Evolution of the upper mantle beneath Southeast Australia: geochemical evidence from peridotite xenoliths in Mount Leura basanite. Earth Planet Sci Lett 93: 195–209

Francis D (1987) Mantle-melt interaction recorded in spinel lherzolite xenoliths from the Alligator Lake volcanic complex, Yukon, Canada. J Petrol 28: 569–597

Frey FA, Prinz M (1978) Ultramafic inclusions from San Carlos, Arizona: petrologic and geochemical data bearing on their petrogenesis. Earth Planet Sci Lett 38: 129–176

Gallagher K, Hawkesworth CJ (1992) Dehydration melting and the generation of continental flood basalts. Nature 258: 57–59

Granet M, Wilson M, Achauer U (1995) Imaging a mantle plume beneath the French Massif Central. Earth Planet Sci Lett 136: 281–296

Green TH, Adam J, Sie SH (1992) Trace element partitioning between silicate minerals and carbonatite at 25 kbar and application to mantle metasomatism. Mineral Petrol 46: 179–184

Hart SR, Dunn T (1993) Experimental clinopyroxene/melt partitioning for 24 trace elements. Contrib Mineral Petrol 113: 1–8

Hauri EH, Hart SR (1994) Constraints on melt migration from mantle plumes: a trace element study of peridotite xenoliths from Savai'i, Western Samoa. J Geophys Res 99: 24301–24321

Hauri EH, Shimizu N, Dieu JJ, Hart SR (1993) Evidence for hotspot-related carbonatite metasomatism in the oceanic upper mantle. Nature 365: 221–227

Hawkesworth CJ, Kempton PD, Rogers NW, Elam RM, van Calsteren PW (1990) Continental mantle lithosphere, and shallow level enrichment processes in the Earth's mantle. Earth Planet Sci Lett 96: 256–268

Hirose K (1997) Melting experiments on lherzolite KLB-1 under hydrous conditions and generation of high-magnesian andesitic melts. Geology 25: 42–44

Irving AJ, Frey FA (1984) Trace element abundances in megacrysts and their host basalts: constraints on partition coefficients and megacryst genesis. Geochim Cosmochim Acta 48: 1201–1221

Jacques AL, Green DH (1980) Anhydrous melting of peridotites at 0–15 kbar pressure and the genesis of tholeiitic basalts. Contrib Mineral Petrol 73: 287–310

Johnson KTM, Dick HJB, Shimizu N (1990) Melting in the oceanic upper mantle: an ion microprobe study of diopsides in abyssal peridotites. J Geophys Res 95: 2661–2678

Johnston ST, Wynne PJ, Francis D, Hart CJR, Enkin RJ, Engbretson DC (1996) Yellowstone in Yukon: the late Cretaceous Carmacks group. Geology 25: 42–44

Jordan TH (1979) Mineralogies, densities and seismic velocities of garnet lherzolites and their geophysical implications. In: Boyd FR, Meyer HOA (eds) The mantle sample: inclusions in kimberlites and other volcanics. Proc 2nd Int Kimberlite Conf, 2, Am Geophys Union pp 1–14

Karato Shun-ichiro (1993) Importance of anelasticity in the interpretation of seismic tomography. Geophys Res Lett 20: 1623–1626

Kelemen PB, Dick HJB, Quick JE (1992) Formation of harzburgite by pervasive melt/rock reaction in the upper mantle. Nature 358: 635–641

Maaløe S, Aoki K (1977) The major element composition of the upper mantle estimated from the composition of lherzolites. Contrib Mineral Petrol 63: 161–173

McDonough WF, Frey FA (1989) Rare earth elements in upper mantle rocks. In: Lipin BR, Mckay (eds) Geochemistry and mineralogy of rare earth elements. (Reviews in mineralogy, 21) Mineral Soc Am, Washington, DC, pp 99–146

McDonough WF, Stosch H-G, Ware NG (1992) Distribution of titanium and the rare earth elements between peridotitic minerals. Contrib Mineral Petrol 110: 321–328

Mysen BO, Kushiro I (1977) Compositional variations of coexisting phases with degree of melting of peridotite in the upper mantle. Am Mineral 62: 843–865

Nadeau S, Pineau F, Javoy M, Francis D (1990) Carbon concentrations and isotopic ratios in fluid-inclusion-bearing upper-mantle xenoliths along the northwestern margin of North America. Chem Geol 81: 271–297

Olafsson M, Eggler DH (1983) Phase relations of amphibole, amphibole-carbonate and phlogopite-carbonate peridotite: petrologic constraints on the asthenosphere. Earth Planet Sci Lett 64: 305–315

Peslier AH, Reisberg L, Carignan J, Ludden J, Francis D, Shi L (1997) Re-Os systematics of the lithospheric mantle under the Canadian Cordillera (abstract). Terra Abstr EUG: 82–83

Prescott J (1983) Petrogenesis of ultramafic xenoliths from the Canadian Cordillera and Alaska (unpublished). MSc thesis, McGill University

Rampone E, Bottazzi P, Ottolini L (1991) Complementary Ti and Zr anomalies in orthopyroxene and clinopyroxene from mantle peridotites. Nature 354: 518–520

Ranalli G (1980) Rheological properties of the upper mantle in Canada from olivine microrheology. Can J Earth Sci 17: 1499–1505

Ringwood AE (1975) Composition and petrology of the Earth's mantle. McGraw-Hill

Roden MF, Shimizu N (1993) Ion microprobe analyses bearing on the composition of the upper mantle beneath the Basin and Range and Colorado plateau provinces. J Geophys Res 98: 14091–14108

Sachtleben Th, Seck HA (1981) Chemical control of Al-solubility in orthopyroxene and its implications on pyroxene geothermometry. Contrib Mineral Petrol 78: 157–165

Schiano P, Clocchiatti R, Shimizu N, Weis D, Mattielli N (1994) Cogenetic silica-rich and carbonate-rich melts trapped in mantle minerals in Kerguelen ultramafic xenoliths: implications for metasomatism in the oceanic upper mantle. Earth Planet Sci Lett 123: 167–178

Sen G, Frey FA, Shimizu N, Leeman WP (1993) Evolution of the lithosphere beneath Oahu, Hawaii: rare earth element abundances in mantle xenoliths. Earth Planet Sci Lett 119: 53–69

Shimizu N (1975) Rare earth elements in garnets and clinopyroxenes from garnet lherzolite nodules in kimberlites. Earth Planet Sci Lett 25: 26–32

Takazawa E, Shimizu N, Frey FA (1994) Development and evolution of the lithospheric mantle: a case study from the Horoman peridotite, Japan (abstract). Mineral Mag 58A: 889–890

Turner S, Hawkesworth C, Gallagher K, Stewart K, Peate D, Mantovani M (1996) Mantle plume, flood basalts, and thermal models for melt generation beneath continents: assessment of a conductive heating model and application to the Parana. J Geophys Res 101: 11503–11518

VanDecar J, James DE, Assumpcao M (1995) Seismic evidence for a fossil mantle plume beneath south America and implications for plate driving forces. Nature 318: 25–31

Wells PRA (1977) Pyroxene thermometry in simple and complex systems. Contrib Mineral Petrol 62: 129–139

Wolfe CJ, Bjarnason IT, VanDecar JC, Solomon SC (1997) Seismic structure of the Iceland mantle plume. Nature 385: 245–247

Woolley AR, Kempe DRC (1989) Carbonatites: nomenclature, average chemical compositions and element distribution. In: Bell K (ed) Carbonatites, genesis and Evolution. Unwin Hyman, London, pp 1–4

Zindler A, Hart SR (1986) Chemical geodynamics. Annu Rev Earth Planet Sci 14: 493–571